

TIME-DOMAIN AND FREQUENCY-DOMAIN METHODS COMBINED IN THE STUDY OF OPEN RESONANCE STRUCTURES OF COMPLEX GEOMETRY

Y. K. Sirenko and L. G. Velychko

Institute of Radiophysics and Electronics
12, Acad. Proskura St., Kharkov, 61085, Ukraine

F. Erden

Gebze Institute of Technology
P.O. 141 41400, Gebze, Kocaeli, Turkey

Abstract—The paper discusses the methodological questions arising in the study of open electrodynamic structures of resonance quasi optics via time-domain technique. As demonstrated, all of the interesting physical characteristics inherent in these objects (including the objects with various frequency-selective elements) can be obtained through the numerical solution of the relevant model initial boundary-value problems. For the first time, a finite difference method equipped with the exact local ‘absorbing’ conditions on artificial boundaries has been applied for the solution of this kind of open problems. The results of the computational experiments performed have verified the possibility of the efficient selection of oscillations in dispersive open resonators with diffraction gratings, among them the resonators with gratings operating in the quasitotal nonspecular reflection mode.

1 Introduction

2 OR of Classical Geometry

3 Dispersive Resonators with Gratings

4 Conclusions

References

1. INTRODUCTION

Many authors (A. G. Fox, T. Li, G. D. Boyd, V. P. Bykov, V. A. Yepishin, Ye. I. Nefedov, C. W. Erickson, T. T. Fong, R. F. Harrington, and others) have contributed in the study on open resonators (OR) in frequency domain. For example, a great body of interesting information has been obtained owing to a waveguide concept of the processes in open oscillating systems suggested and developed by L. A. Weinstein [1]. However, if the mirrors possess a complex geometry, even the most fruitful approach (see works of V. P. Shestopalov, V. N. Koshparionok, P. N. Melezhik, and A. Ye. Poyedinchuk) provides nothing but analytical description of the spectrum (discreteness, finite multiplicity and other general characteristics resulting from Fredholm's theorem for compact finite-meromorphic operator-functions), qualitative assessment of its components, and approximate estimation of the components' action on the formation of transient characteristics of an OR. As to the time-domain technique, it has been little used for the analysis of composite open structures with resonance elements. In this connection, mention may be made of Chapter 16 'Microcavity ring resonators' in [2] as of the well-thought-out approach to the above problem.

In this paper, we demonstrate the considerable possibilities of the integration of the frequency-domain and the time-domain methods in the analysis of complex resonance structures. Using OR with cylindrical mirrors and OR with diffraction gratings as examples, we treat a number of methodological problems arising in the approach suggested.

2. OR OF CLASSICAL GEOMETRY

The computational experiments discussed below were carried out with the use of the algorithm developed in [3]. The initial-boundary value problem

$$\left\{ \begin{array}{l} \left[-\varepsilon(g) \frac{\partial^2}{\partial t^2} - \sigma(g) \frac{\partial}{\partial t} + \frac{\partial^2}{\partial z^2} + \frac{\partial^2}{\partial y^2} \right] U(g, t) = F(g, t), \quad t > 0, \quad g \in \mathbf{Q}_L \\ U(g, t) \Big|_{t=0} = \varphi(g), \quad \frac{\partial}{\partial t} U(g, t) \Big|_{t=0} = \psi(g) \\ U(g, t) = E_x, \quad \frac{\partial}{\partial t} H_y = -\frac{1}{\eta_0} \frac{\partial}{\partial z} E_x, \quad \frac{\partial}{\partial t} H_z = \frac{1}{\eta_0} \frac{\partial}{\partial y} E_x, \\ E_y = E_z = H_x \equiv 0 \\ \mathbf{Q}_L = \{g = \{y, z\} \in \mathbf{R}^2 : L_4 < y < L_3; L_2 < z < L_1\} \end{array} \right. \quad (1)$$

for the E -polarized field $U(g, t)$ is discretized by the finite-difference method on a rectangular grid of Cartesian coordinates y and z . Here and in Fig. 1, $\sigma = \sigma_0 \eta_0$, $\varepsilon(g)$ and $\sigma_0(g)$ are the relative permittivity and conductivity of the medium inhomogeneities respectively; $\eta_0 = (\mu_0/\varepsilon_0)^{1/2}$ is the impedance of free space; the functions F , φ , ϕ , σ , and $\varepsilon - 1$ are finite in \mathbf{R}^2 , while their supports belong to \mathbf{Q}_L over the time interval $0 \leq t \leq \tilde{T}$.

When closing the rectangular analysis domain \mathbf{Q}_L by the boundary $\mathbf{L} = \overline{\mathbf{Q}_L} \setminus \mathbf{Q}_L$ with $\overline{\mathbf{Q}_L}$ being the closure of \mathbf{Q}_L , the following exact local ‘absorbing’ conditions are used:

$$\left\{ \begin{array}{l} \left[\frac{\partial}{\partial t} \pm \frac{\partial}{\partial z} \right] U(g, t) = \frac{2}{\pi} \int_0^{\pi/2} \frac{\partial V_1(g, t, \varphi)}{\partial t} \sin^2 \varphi d\varphi, \quad z \begin{cases} \geq L_1 \\ \leq L_2 \end{cases} \\ \left[\frac{\partial^2 V_1(g, t, \varphi)}{\partial t^2} - \frac{\partial^2 W_1(g, t, \varphi)}{\partial y^2} \right] = 0, \\ \frac{\partial V_1(g, t, \varphi)}{\partial t} \Big|_{t=0} = V_1(g, t, \varphi) \Big|_{t=0} = 0, \\ W_1(g, t, \varphi) = V_1(g, t, \varphi) \cos^2 \varphi + U(g, t) \end{array} \right. \quad (2)$$

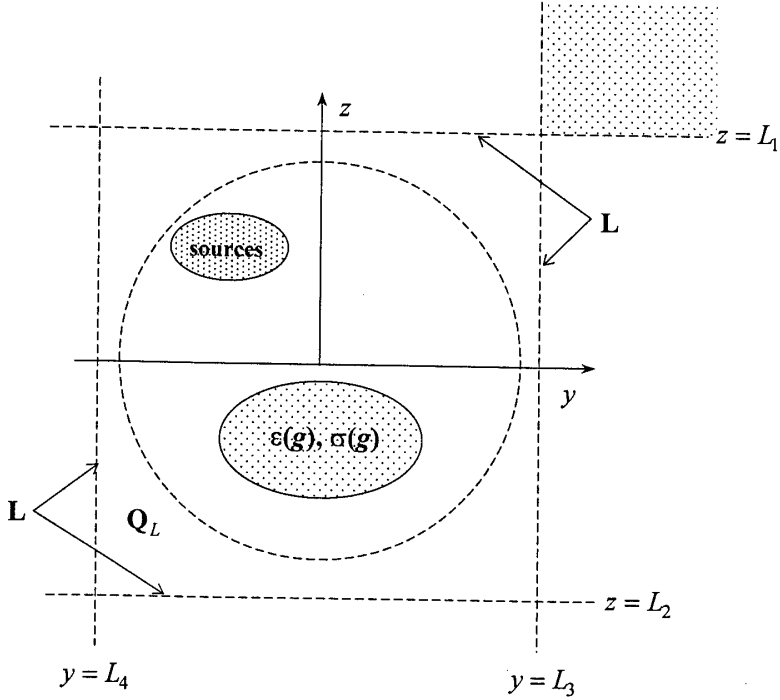


Figure 1. Geometry of the problem (1).

$$\left\{ \begin{array}{l} \left[\frac{\partial}{\partial t} \pm \cos \varphi \frac{\partial}{\partial y} \right] W_1(g, t, \varphi) \\ = \frac{2 \cos \varphi}{\pi} \int_0^{\pi/2} \frac{\sin^2 \gamma}{\cos^2 \varphi + \sin^2 \varphi \cos^2 \gamma} \frac{\partial W_2(g, t, \gamma)}{\partial t} d\gamma, \quad y \begin{cases} \geq L_3 \\ \leq L_4 \end{cases} \\ \left[\frac{\partial}{\partial t} \pm \cos \varphi \frac{\partial}{\partial z} \right] W_2(g, t, \varphi) \\ = \frac{2 \cos \varphi}{\pi} \int_0^{\pi/2} \frac{\sin^2 \gamma}{\cos^2 \varphi + \sin^2 \varphi \cos^2 \gamma} \frac{\partial W_1(g, t, \gamma)}{\partial t} d\gamma, \quad z \begin{cases} \geq L_1 \\ \leq L_2 \end{cases} \end{array} \right. \quad (3)$$

$$\left\{ \begin{array}{l} \left[\frac{\partial}{\partial t} \pm \frac{\partial}{\partial y} \right] U(g, t) = \frac{2}{\pi} \int_0^{\pi/2} \frac{\partial V_2(g, t, \varphi)}{\partial t} \sin^2 \varphi d\varphi, \quad y \begin{cases} \geq L_3 \\ \leq L_4 \end{cases} \\ \left[\frac{\partial^2 V_2(g, t, \varphi)}{\partial t^2} - \frac{\partial^2 W_2(g, t, \varphi)}{\partial z^2} \right] = 0, \\ \frac{\partial V_2(g, t, \varphi)}{\partial t} \Big|_{t=0} = V_2(g, t, \varphi) \Big|_{t=0} = 0. \\ W_2(g, t, \varphi) = V_2(g, t, \varphi) \cos^2 \varphi + U(g, t) \end{array} \right. \quad (4)$$

The inclusion of these conditions into original problem (1) does not change the problem qualitatively and does not distort its solution (the relevant analysis has been presented in [4, 5]). The problem of corner points of the boundary L has been resolved rigorously in the framework of relationships (2)–(4) (here $V_j(g, t, \varphi)$, $j = 1, 2$ are certain auxiliary functions).

Throughout this paper the boundaries of the analysis domain \mathbf{Q}_L coincide with the boundaries of the figures with the time dependence of the electric field intensity $U(g, t) = E_x$ at the points $g = \{y, z\} \in \mathbf{Q}_L$.

The parameters of the scatterers ($\varepsilon(g)$ and $\sigma(g)$), the ‘current’ sources ($F(g, t)$), and the ‘momentary’ sources ($\varphi(g)$ and $\psi(g)$) are specified by step-functions like $\chi[f_1(g)]\chi[f_2(g)] \dots \chi[f_m(g)]$, where χ is the Heaviside function. All metal parts of the resonators, radiators, etc. are assumed to be copper; all dimensions are given in centimeters. For example, the OR mirrors with spectral characteristics presented in Figures 2–4 are described by the following functions:

$$\sigma(g) = 2.19 \cdot 10^8 \chi[5 - |y|] \chi[4 - |z|] \chi \left[z^2 + (|y| + 4.5)^2 - 9^2 \right]$$

(an OR with a confocal geometry (Figs. 3, 4); the radius R of the mirrors and the mirror spacing L along the principal resonator axis are equal to 9.0),

$$\sigma(g) = 2.19 \cdot 10^8 \chi[5 - |y|] \chi[4 - |z|] \chi \left[z^2 + (|y| + 6.5)^2 - 11^2 \right]$$

(an OR with an ‘under-confocal’ geometry; $R = 11.0$ and $L = 9.0$), and

$$\sigma(g) = 2.19 \cdot 10^8 \chi[5 - |y|] \left\{ \chi[4 - |z|] \chi \left[z^2 + (y - 4.5)^2 - 9^2 \right] + \chi[4 - |z + 2|] \chi \left[(z + 2)^2 + (y + 4.5)^2 - 9^2 \right] \right\}$$

(an axis discontinuity in a confocal OR (Fig. 4b); the center distance in a vertical direction is equal to 2.0).

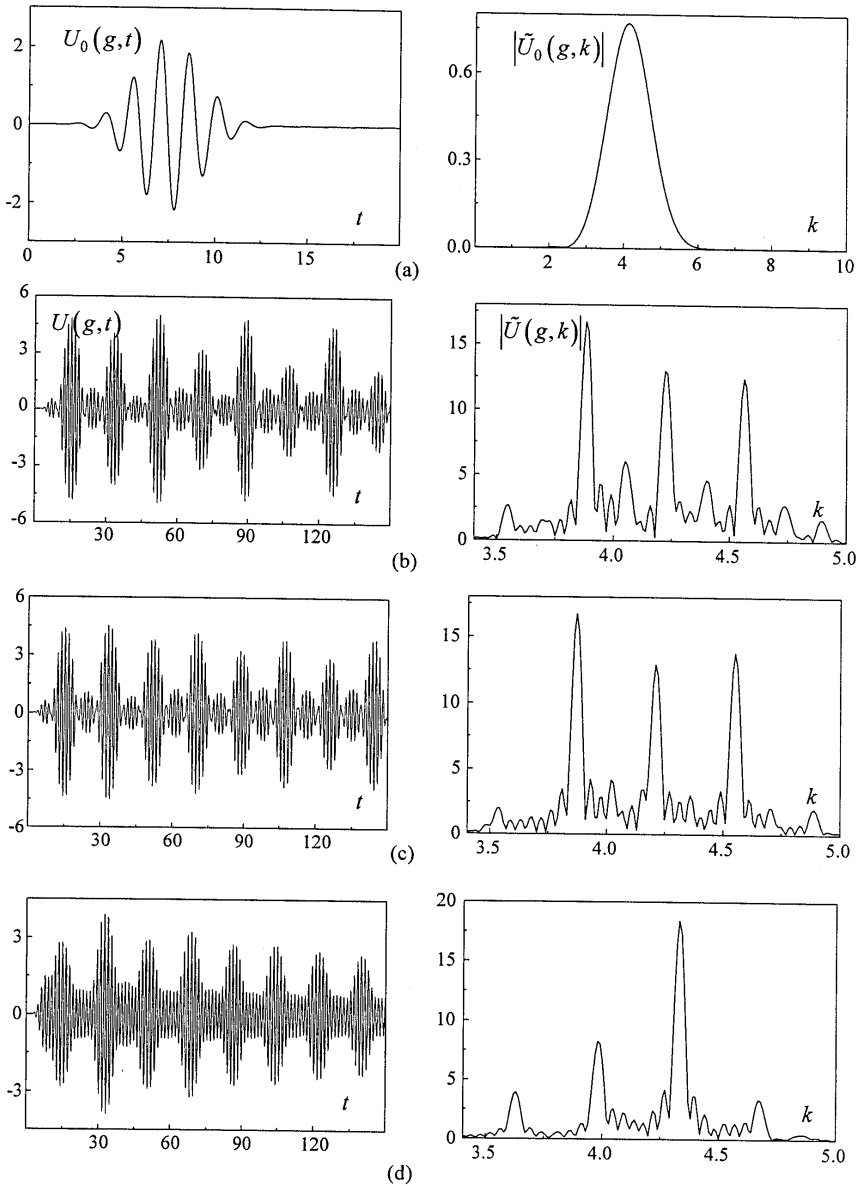


Figure 2. Spectral characteristics of the source (a), of the resonators with confocal (b) and ‘under-confocal’ (c) geometry, and of the resonator with the principal axis discontinuity (d): $\tilde{k} = 4.2$; $g = \{0; 0\}$ (a) and $g = \{0.2; 0.2\}$ (b–d).

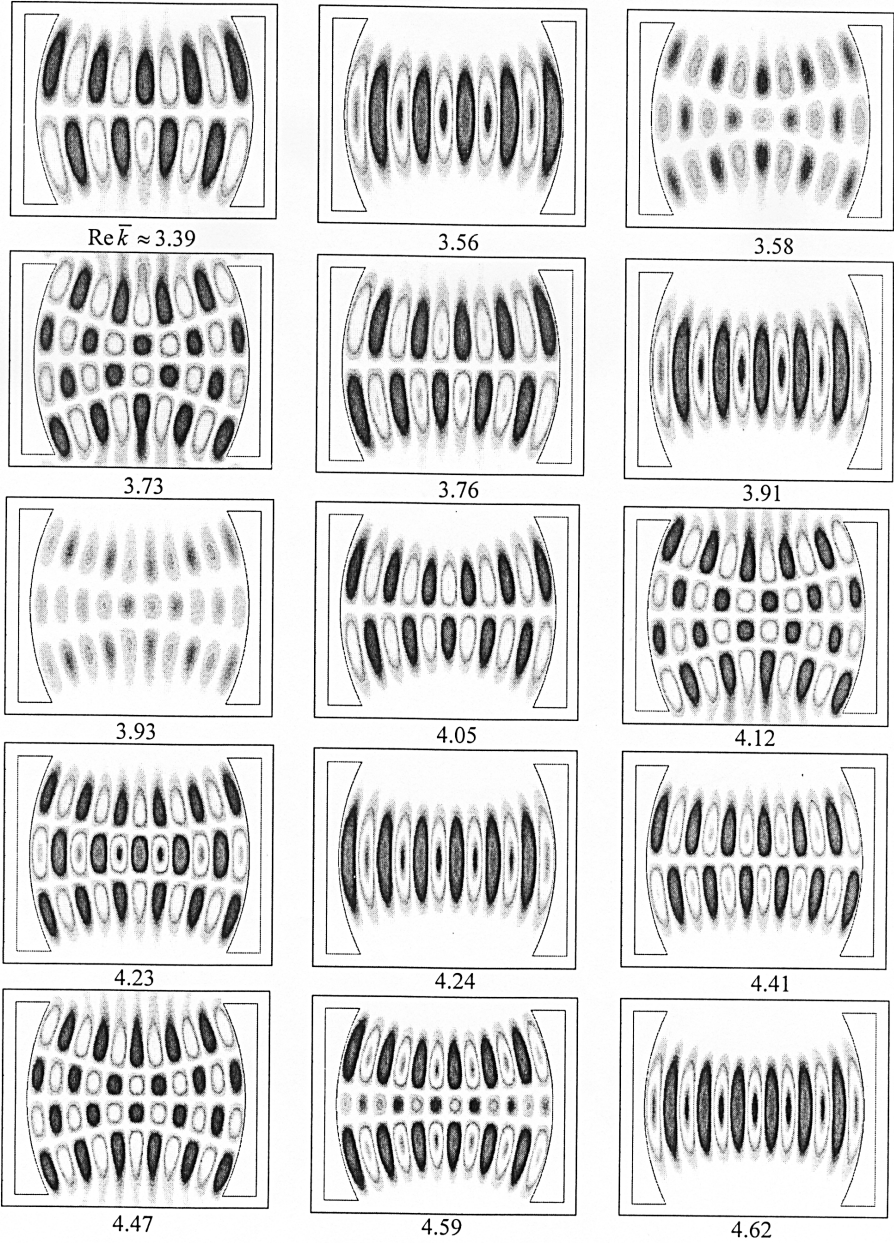


Figure 3. Configuration, the order (in frequency) and approximate values of $\text{Re } \bar{k}$ for high- Q free oscillations in the confocal resonator.

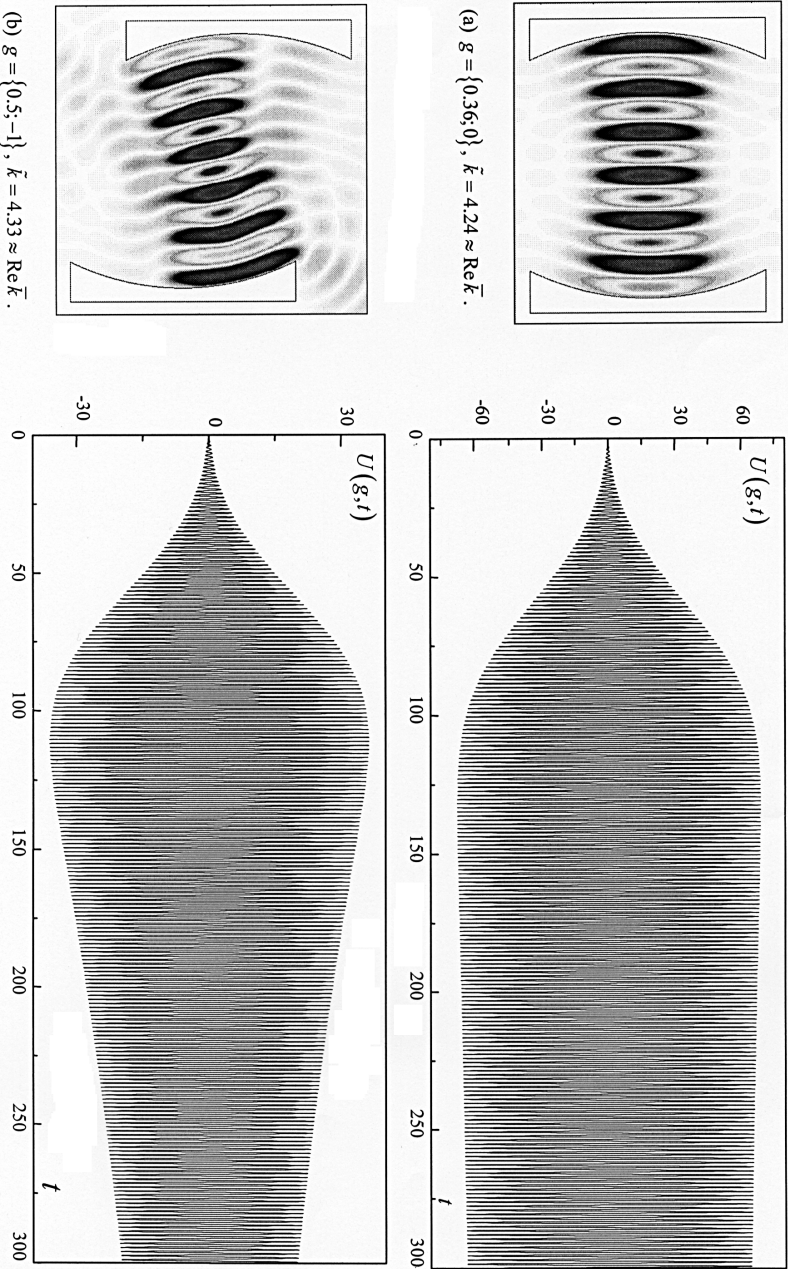


Figure 4. Oscillations of the same type in the confocal resonator (a) and the resonator with the principal axis discontinuity (b).

The source exciting an OR as well as the observation time interval $0 \leq t \leq \tilde{T}$ should correlate with the purpose of the particular problem. An example will make this clear. In a set of the experiments discussed in the paper, the ‘current’ source has the form

$$F(g, t) = 10\chi[3.5 - |y|]\chi[1.5 - |z+1|] \cos(\beta_1 \tilde{k}y + \beta_2) \cos(\beta_3 \tilde{k}z + \beta_4) \\ \times \exp[-(t - T)^2/4\tilde{\alpha}^2] \cos[\tilde{k}(t - T)]. \quad (5)$$

This function possesses seven free parameters: \tilde{k} , $\tilde{\alpha}$, T , and β_j , $j = 1, 2, 3, 4$. The first parameter (\tilde{k}) specifies an amplitude center of the primary signal in the spectral domain, i.e. the maximal absolute value of the function

$$\tilde{U}_0(g, k) = \frac{1}{2\pi} \int_{-\infty}^{\infty} U_0(g, t) e^{ikt} dt \equiv F[U_0(g, t)](k) \leftrightarrow U_0(g, t) \quad (6)$$

with $U_0(g, t)$ being the field generated by the source $F(g, t)$ in R^2 space with $\varepsilon(g) \equiv 1$ and $\sigma(g) \equiv 0$. This parameter, in combination with $\tilde{\alpha}$, determines the frequency band $[\tilde{k} - b/\tilde{\alpha}; \tilde{k} + b/\tilde{\alpha}]$, where the normalized spectral amplitude of the pulse $U_0(g, t)$ ($|\tilde{U}_0(g, k)|/|\tilde{U}_0(g, \tilde{k})|$) does not go below some value γ . In the t -axis, the signal $U_0(g, t)$ ‘occupies’ an interval $T - c\tilde{\alpha} \leq t \leq T + c\tilde{\alpha}$ such that the value $|U_0(g, t)|/|U_0(g, T)|$ outside this interval does not exceed γ . The coefficients b and c deduced from the familiar relationship

$$\frac{1}{2} e^{iT\tilde{k}} \left[e^{-\tilde{\alpha}^2(k-\tilde{k})^2} + e^{-\tilde{\alpha}^2(k+\tilde{k})^2} \right] \leftrightarrow \frac{\pi^{1/2}}{\alpha} e^{-(t-T)^2/4\tilde{\alpha}^2} \cos[\tilde{k}(t - T)]$$

are listed in the Table 1 for several fixed values of γ . The parameters β_j allow tuning the source to generating oscillations of the particular symmetry class or, on the contrary, oscillations of all types. With the help of these parameters we will also impart a definite structure to $U_0(g, t)$ (for example, a structure of a near-plane wave with the wavelength $2\pi/\tilde{k}$).

Now we dwell on the requirements imposed on the above-listed parameters when analyzing spectral characteristics of an OR (see Fig. 2). It is apparent that \tilde{k} should be made coincident with the center of the frequency range while $\tilde{\alpha}$ is to be chosen so that the level of the normalized spectral amplitudes of $U_0(g, t)$ within this range could not exceed 0.1 or, better still, 0.5 (to prevent noticeable distortions of some ‘ideal’ picture, which is observed when $|\tilde{U}_0(g, k)|$ remains the same

Table 1.

	$\gamma = 0.001$	$\gamma = 0.01$	$\gamma = 0.1$	$\gamma = 0.5$
$b \approx$	2.63	2.14	1.52	0.83
$c \approx$	5.25	4.29	3.04	1.66

over the whole frequency range). The left boundary of the interval $T - c\tilde{\alpha} \leq t \leq T + c\tilde{\alpha}$ is placed at the point $t = 0$ in an effort to cut the computation time \tilde{T} . For the expected spectral characteristics of the source to be conserved, $|U_0(g, 0)|$ ($U_0(g, t) = 0$, $t < 0$) must correspond to $0.001 \leq \gamma \leq 0.01$. This requirement along with the parameter $\tilde{\alpha}$ determines the efficient signal length $0 \leq t \leq 2T$ and, hence, the delay time T . At this point our interest is oscillations of every mode. Then, the field $U_0(g, t)$ should not be orthogonal to any one of the possible free oscillations in the system (this requirement is controlled by β_j). The efficiency of the excitation of all spectral components of the total field $U(g, t)$ is largely depended upon the spatial dimensions of the source; by extending the range of g values where $F(g, t) \neq 0$ we can substantially reduce the computation time. The lower limit ($\tilde{T} = 5T$) of possible values of \tilde{T} is governed by the following evident requirement: in a time $0 \leq t \leq \tilde{T}$, the OR has to spend the time $0 \leq t \leq 2T$ operating in the forced oscillation mode, then, to get rid (at the cost of the radiation into free space) of spectral components that are incapable of forming stable oscillations in the resonator ($2T \leq t \leq 3T$), and, finally, to provide a way for high- Q oscillations to show themselves against a background of low- Q oscillations ($3T \leq t \leq 5T$). In this case, the analysis of spectral characteristics of an OR in a frequency band reduces to the following operations: the calculation of $U(\tilde{g}, t)$ at the point \tilde{g} in the resonator as a function of time $t \in [0; \tilde{T}]$ and, then, the analysis of the Fourier transform $\tilde{U}(\tilde{g}, k) \leftrightarrow U(\tilde{g}, t)$ (formula (6): $U(\tilde{g}, t)$ is assumed to be equal to zero outside the interval $t \in [0; \tilde{T}]$).

When analyzing the isolated oscillations $\tilde{U}_n(g, \bar{k}_n)$ separated from the complete spectrum of the OR, the interval $[k - b/\tilde{\alpha}; k + b/\tilde{\alpha}]$ ($k \approx \text{Re}\bar{k}_n$) has to involve no resonance points adjacent to $\text{Re}\bar{k}_n$ while a magnitude of spectral amplitudes of $U_0(g, t)$ should be insignificant at the ends of this interval. It is obvious that this requirement can be weakened considerably through using sources of definite symmetry class.

In the frequency range [3.4, 5.0] the normalized spectral amplitudes of the pulse $U_0(g, t)$ (Fig. 2a) generated by the source (5)

with $\tilde{\alpha} = 1$, $T = 6$, $\beta_1 = 1$, $\beta_2 = \pi/4$, and $\beta_3 = \beta_4 = 0$ do not go below 0.3. During the time $\tilde{T} = 150$, all resonators of classical configuration mentioned above extract efficiently the spectral components associated with the high- Q quasi-harmonic oscillations (sharp peaks of $|\tilde{U}(g, k)|$ in Fig. 2b–d). The parameters of the amplitude centers defining the eigenfrequencies of the H_{0n1} -oscillations in the resonator spectra are near-identical even under sizable deviations of R/L from the unity for confocal, ‘under-confocal’, and ‘over-confocal’ ($R < L$) geometries. Only the distinct capacity for sustaining the oscillations with two or more field variations along the vertical axis is easily observable: it is considerably greater for confocal resonators. As to the resonator with the axis discontinuity, its spectrum possesses a greater number of distinctive features: the H_{0nm} -oscillations with $m \geq 2$ become unstable while the associated spectral amplitudes of $U(g, t)$ are reduced to the background level. However, even with small intersection area of mirror projections, this kind of resonator is capable to sustain high- Q free H_{0n1} -oscillations (see, for example, Fig. 4b).

From the spikes of $|\tilde{U}(g, k)|$, the approximate values of $\text{Re}\bar{k}$ (\bar{k} stands for the resonator eigenfrequency) are easily determined for every high- Q free oscillation that is sustained by the given OR. These values can be refined and the field configuration of the related free oscillations can be visualized by the application of the peculiarly adapted source $F(g, t)$. The source parameters (Fig. 3, the ‘confocal’ geometry) were chosen with regard to the oscillation mode and its Q -factor. In some instances, two or three related ‘iterations’ were called for. If a quasimonochromatic component associated with the free oscillation $\tilde{U}_n(g, \bar{k}_n)$ dominates in the field $U(g, t)$ after termination of the source operation, the changes of the field intensity are determined [6] by the factor $\exp(-|\text{Im}\bar{k}_n|t)$. This fact allows calculating both $\text{Im}\bar{k}_n$ and the Q -factor $Q_n = \text{Re}\bar{k}_n/2|\text{Im}\bar{k}_n|$ of the corresponding free oscillation with the use of the results similar to those presented in Fig. 4. The source (5) with $\tilde{\alpha} = 20$, $T = 60$, $\beta_1 = 1$, $\beta_3 = \beta_4 = 0$, $\beta_2 = \pi/2$ (Fig. 4a) and $\beta_2 = \pi/4$ (Fig. 4b) provides all necessary conditions for this type of calculation. Evidently, the total observation time \tilde{T} can be increased, if highly accurate $\text{Im}\bar{k}_n$ is needed.

3. DISPERSIVE RESONATORS WITH GRATINGS

Now we apply the approach presented in the previous section to the analysis of OR with diffraction gratings. It should be stressed that the computational experiment has to start from the clear view of all special features in the ‘operation’ of the dispersive element during

forming high- Q oscillations in a structure. We begin with the analysis of spectral characteristics of the Fabry-Perot resonator (Figs. 5, 6): a resonator with plane parallel mirrors

$$\sigma(g) = 2.19 \cdot 10^8 \chi[4 - |y|] \{ \chi(z + 0.3) \chi(-z) + \chi(10.3 - z) \chi(z - 10) \} \quad (7)$$

(the resonator width is equal to 8.0 while the mirror spacing is equal to 10.0). A source

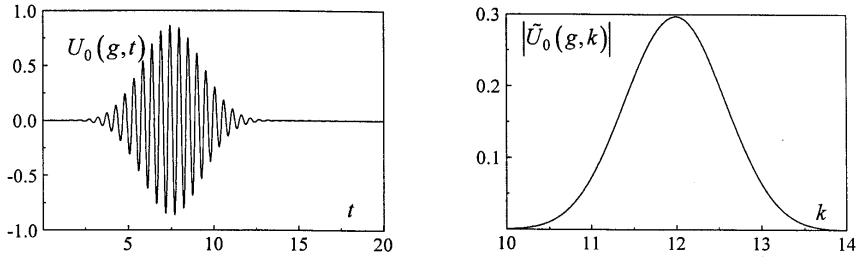
$$F(g, t) = 10 \chi[3 - |y|] \chi(z - 2) \chi(8 - z) \cos(\tilde{k}z + \beta) \cdot \exp \left[-(t - T)^2 / 4\tilde{\alpha}^2 \right] \cos[\tilde{k}(t - T)] \quad (8)$$

excites in the structure nothing but symmetrical oscillations with respect to the axis $y = 0$. The normalized spectral amplitudes of the relevant field $U_0(g, t)$ for $\tilde{\alpha} = 1$ and $T = 6$ in the frequency range $[\tilde{k} - 1, \tilde{k} + 1]$ do not go below a level $\gamma = 0.23$ (Fig. 5a). In the calculation of frequency characteristics $\tilde{U}(g, k) \leftrightarrow U(g, t)$, $0 \leq t \leq \tilde{T} = 150$ (see, for example, Fig. 5b and Fig. 6b), these parameters of the function $F(g, t)$ ($\beta = 0.08\tilde{k}$ for $\tilde{k} = 8$ and $\tilde{k} = 14$; $\beta = 0.08\tilde{k} + \pi/4$ for $\tilde{k} = 10$ and $\tilde{k} = 12$) remain the same. The tuning of the source to the analysis of the isolated high- Q oscillations (for example, $H_{0,1,38}$ -oscillation in Fig. 5c and $H_{0,1,26}$ -oscillation in Fig. 6a) is achieved through increasing the magnitude of the parameters $\tilde{\alpha}$, T , and \tilde{T} up to the values 20, 80, and 300, respectively. The coordinates $y = 0$ and $z = 10 - \pi/2\tilde{k}$ of the points g (the resonator axis; the distance from the upper mirror is equal to one fourth of the probing wavelength) where time characteristics of $U(g, t)$ are determined, remain constant and will be changed in the case of the resonator with two selective mirrors.

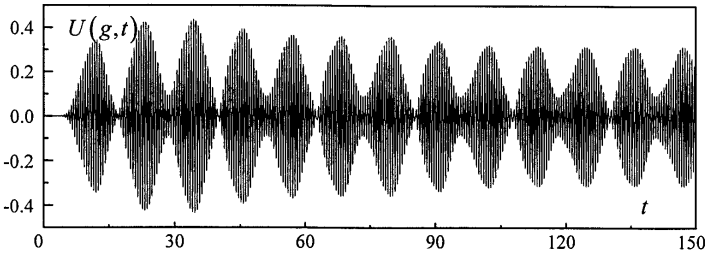
Let us replace the bottom mirror of the resonator (7) with a metal grating (Fig. 6a)

$$\sigma(g) = 2.19 \cdot 10^8 \chi[4 - |y|] \{ \chi(-z) \chi(z + 0.235) \chi[\cos(2\pi y/0.543) - \cos(\pi/2)] + \chi(-z - 0.235) \chi(z + 0.535) \}$$

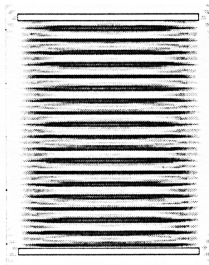
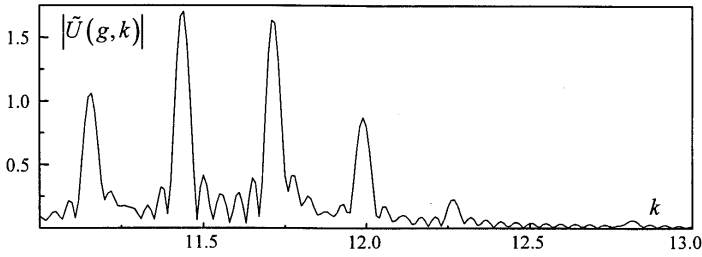
Here the following grating parameters have been used: the period $l = 0.543$, the height $h = 0.235$, and the slot width $d = 0.5l$. The reflection area coincides with the half-plane $z > 0$. The upper limit of the single-wave range [6, 7] for the corresponding perfectly conducting infinite structure excited by a normally incident plane wave ($\alpha = 0$; the angle of incidence is counted of anticlockwise from the z -axis) is determined by the parameter $k_{\pm 1} = 11.57$ (or, by the frequency parameter $\kappa_{\pm 1} = l/\lambda = lk_{\pm 1}/2\pi = 1$). In this range $|a_0(k)| = 1$; the value of $\arg a_0(k)$ varies between 180° and 260° (where $a_n(k)$ are



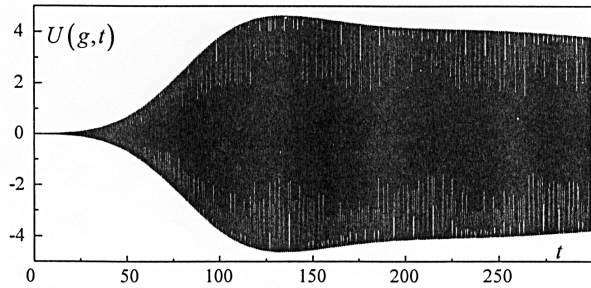
(a)



(b)



$\bar{k} = 11.44 \approx \text{Re} \bar{k}; t = 240$



(c)

Figure 5. On the analysis of open dispersive resonators: $a - \bar{k} = 12, g = \{0; 4.72\}$; $b - \bar{k} = 12, g = \{0; 9.87\}$; $c - g = \{0; 9.87\}$.

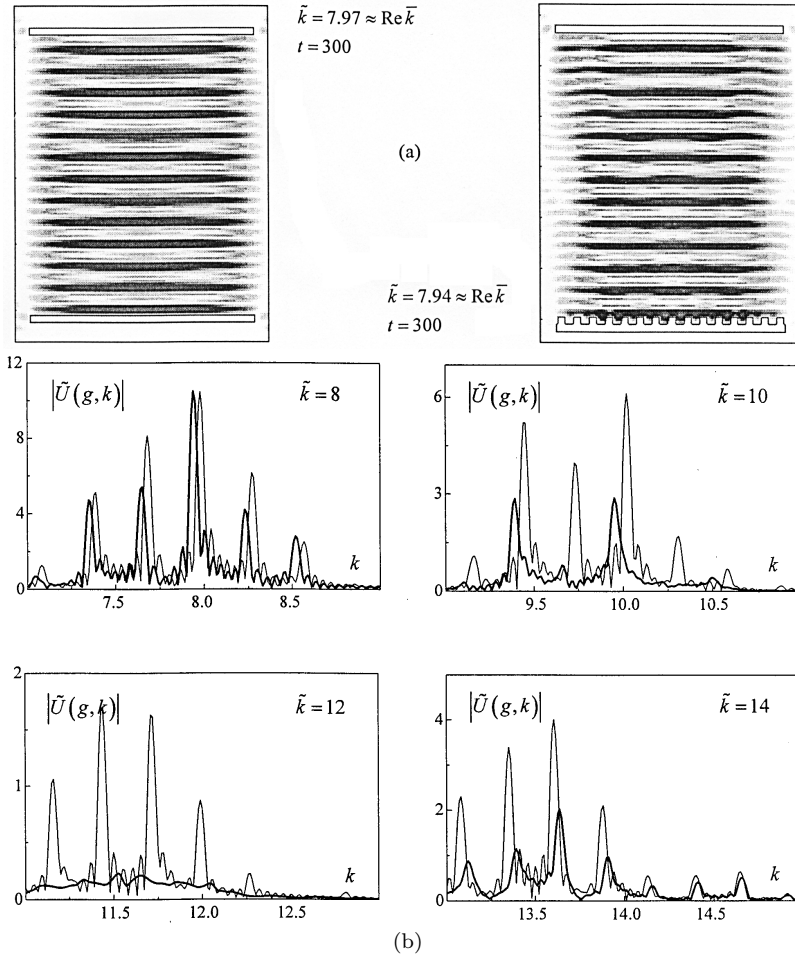


Figure 6. A comparison between spectral characteristics of the Fabry-Perot resonator (thin lines) and the dispersive resonator with a grating (bold lines): $g = \{0; 10 - \pi/2\tilde{k}\}$.

complex amplitudes of spatial harmonics of the field resulting from the excitation of the periodic structure by a plane wave, see Figures 135 and 158 in [7] for amplitude-frequency characteristics of the grating). From the standpoint of an observer stationed in a far-field region, there is no distinction in the ‘operation’ of the grating and the perfectly conducting plane $z = (\pm\pi - \arg a_0)/2k$. In the frequency range $k_{\pm 1} \leq k \leq 13.9$, the efficiency of a specular reflection abruptly falls because of the energy redistribution between the spatial harmonics

with the numbers 0, +1, and -1, then it increases again up to the unity ($k = 17.3$) and so on.

If we start from the assumption of the energy balance relationship for perfect infinite structures [6–8] in an effort to predict a nature of changes in the OR spectrum, the result will be as follows. Up to the threshold point $k_{\pm 1}$, the distribution of spectral amplitudes $|\tilde{U}(g, k)|$ of the field $U(g, t)$ remains mainly unchanged: the resonance frequencies are driven towards the values $\arg a_0 \neq \pi$, being shifted slightly along the k -axis, while Q -factor of the corresponding free oscillations is changed moderately. Beyond the point $k_{\pm 1}$, the ratio between the levels of local amplitude centers of $|\tilde{U}(g, k)|$ for the dispersive resonator and the Fabry-Perot resonator will coincide (with slight deviations) with $|a_0(k)|$.

What actually happens is that the above assumption turns out to be only partially valid (see Fig. 6b): a sharp boundary at the point $k_{\pm 1}$ spreads over the interval $10.0 < k < 13.0$ ($0.86 < \kappa < 1.12$), where the amplitudes $|\tilde{U}(g, k)|$ reduce down to the nonresonant background. The chief cause (Cf. the data presented in Fig. 7a and Fig. 7b) is in the anomalous energy redistribution of the forced oscillations between the regions adjacent to the upper (non-selective) mirror and the bottom (grating) mirror. The relative rise in the intensity of the near-zone field and its efficient radiation into free space is ensured by the ‘trapped’ harmonics, which exhibit a standard behavior (for the spectral domain) in the vicinity of the threshold point $k_{\pm 1}$.

Replace now the bottom plane mirror of the resonator (7) with a finite grating

$$\begin{aligned} \sigma(g) = & 2.19 \cdot 10^8 \chi[4 - |y|] \{ \chi(-y \sin \eta - z \cos \eta) \\ & \times \chi(y \sin \eta + z \cos \eta + 0.26) \chi[\cos(2\pi(y \cos \eta - z \sin \eta)/0.75) \\ & - \cos(0.15\pi)] + \chi(-y \sin \eta - z \cos \eta - 0.26) \\ & \times \chi(y \sin \eta + z \cos \eta + 0.56) \end{aligned} \quad (9)$$

(see Fig. 8a; $\eta = 24.06^\circ$ is the angle of the structure rotation about the point $g = \{0; 0\}$ counted clockwise).

The infinite periodic structure (9) with the parameters $l = 0.75$, $h = 0.26$, and $d = 0.85l$ in the frequency range $8.7 < k < 11.9$ ($1.04 < \kappa < 1.43$), when ‘operating’ in the autocollimation mode on the ‘-1’ spatial harmonic (see [6, 7]), concentrates the energy of the secondary field almost entirely in a plane wave propagating towards the incident direction. These data shown in Fig. 133 in [6] give grounds to suggest the following: if a plane mirror of the Fabry-Perot resonator (7) is replaced with the grating (9) properly oriented in the space (this condition determines the choice of the parameter η), then the modified

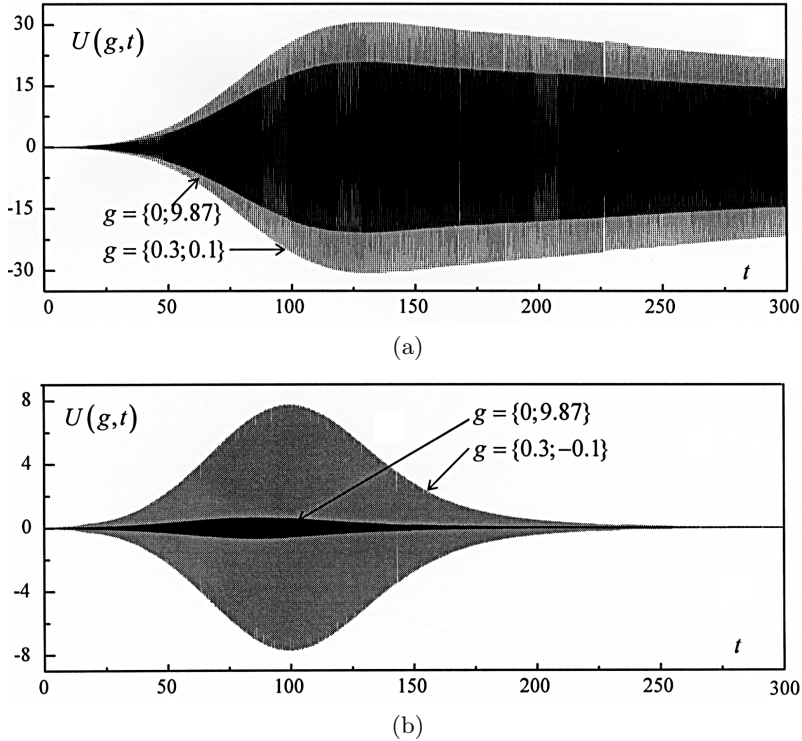


Figure 7. The field intensity near the dispersive resonator mirrors: $a - \tilde{k} = 7.94$; $b - \tilde{k} = 11.52$.

resonator will also sustain high- Q oscillations for $8.7 < k < 11.9$. However, outside this range, the resonator spectrum turns out to be substantially sparse. Figures 8 and 9 confirm this fact. The angle $\alpha = \eta$ corresponds to the frequency $k = 10.27$ of the autocollimation reflection into the grating spatial harmonic with the number -1 . Therefore, a dispersive resonator with spectral curves shown in Fig. 8a replicates (without noticeable distortion) the characteristics of the original resonator in the relevant narrow frequency range. The degree of the excitation of one of the oscillations captured by this band has decreased slightly whereas the other one has increased. Outside this range, the spectrum gradually acquires the form of a nonresonant background: the plane stationary mirror does not allow the frequency properties of the periodic structure, specifically, its capacity for nearly total autocollimation reflection to be fully realized. The situation can be changed in two ways. The first way calls for the continuous spatial

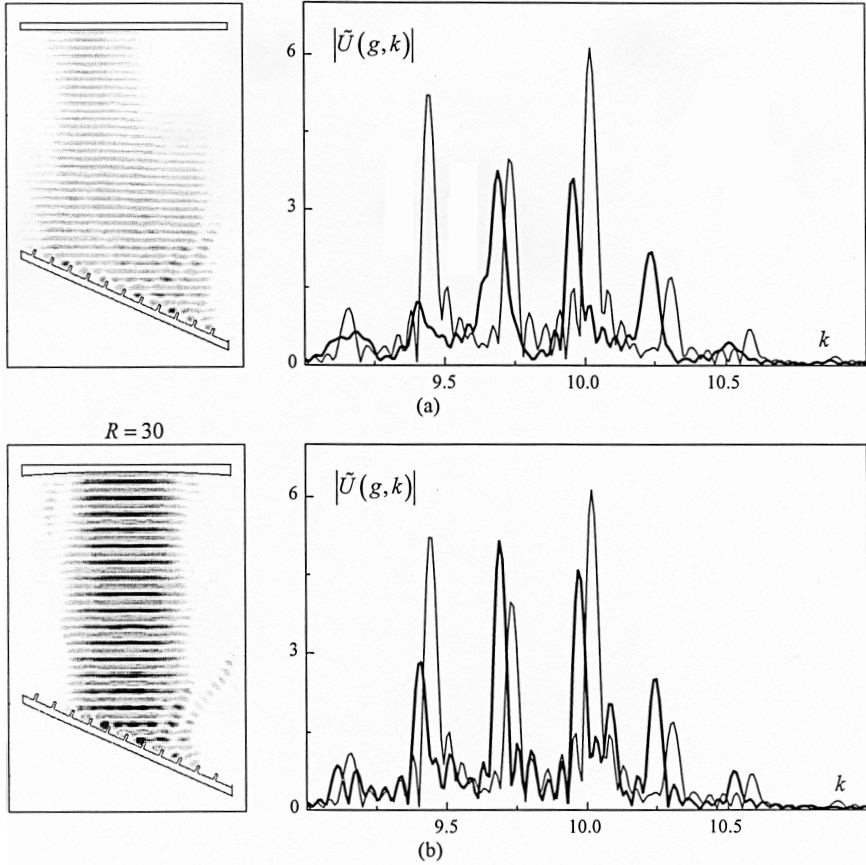


Figure 8. Variations in spectral characteristics of the Fabry-Perot resonator (thin lines) with a grating ‘operating’ in the autocollimation mode in place of the bottom mirror: $\tilde{k} = 10$; $t = 142$; $g = \{0; 9.84\}$.

reorientation of the mirrors according to the condition $2\kappa \sin \alpha = 1$; another way is associated with the replacement of the plane mirror in the cylindrical one

$$\sigma(g) = 2.19 \cdot 10^8 \chi[4 - |y|] \chi(10.3 - z) \chi \left[y^2 + (z + R - 10)^2 - R^2 \right] \quad (10)$$

(see Fig. 8b–11 with R being the radius of a mirror curvature). Comparison characteristics (approximate values of $\text{Re} \tilde{k}$, field configuration, and Q -factor) of the high- Q oscillations retained in the spectrum are presented in Figures 10 and 11. As to the spectrum rarefication outside

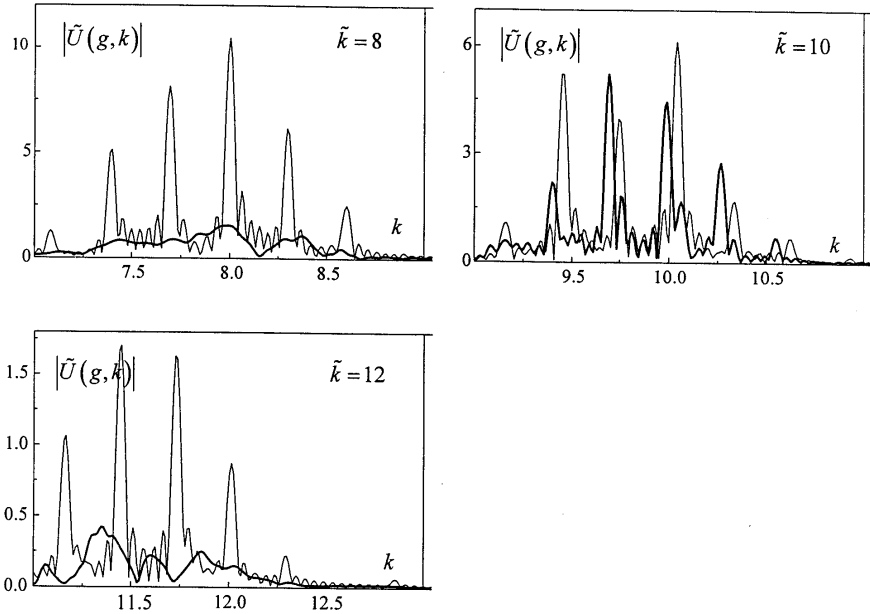


Figure 9. Spectral characteristics of the dispersive resonator (bold lines) and the Fabry-Perot resonator (thin lines) in the frequency range $7 \leq k \leq 13$: $g = \{0; 10 - \pi/2\tilde{k}\}$, $R = 50$.

the ‘principal’ band $9 < k < 11$, the observed effect here is in complete agreement with the expected one (see Fig. 9).

In closing, one additional example can be given (Fig. 12), where both of plane mirrors of the original resonator (7) are replaced with gratings. The distance along the axis $y = 0$ between the bottom mirror (9) and its precise replica, properly positioned in the upper part of the space, remains equal to 10.0. A comparison of the plots given in Figures 9 and 12 (the characteristics of the dispersive resonator (9), (10) with $R = 50$ are duplicated in the bottom fragment by the dotted line) allows the following conclusion: the ‘focusing’ ability of two grating mirrors ‘operating’ in the mode of autocollimation reflection can be considerably greater as compared with two parallel plane mirrors or with the system ‘cylindrical mirror — grating’. The reason is that in this case the condition $2\kappa \sin \alpha = p$, $p = 1, 2, \dots$, is realized automatically, which is necessary for forming stable oscillations according to the scheme ‘incident wave — reflected wave propagating in the opposite direction’. Two grating mirrors resolve the problem of the adoption of narrow-band effects of the total nonspecular reflection

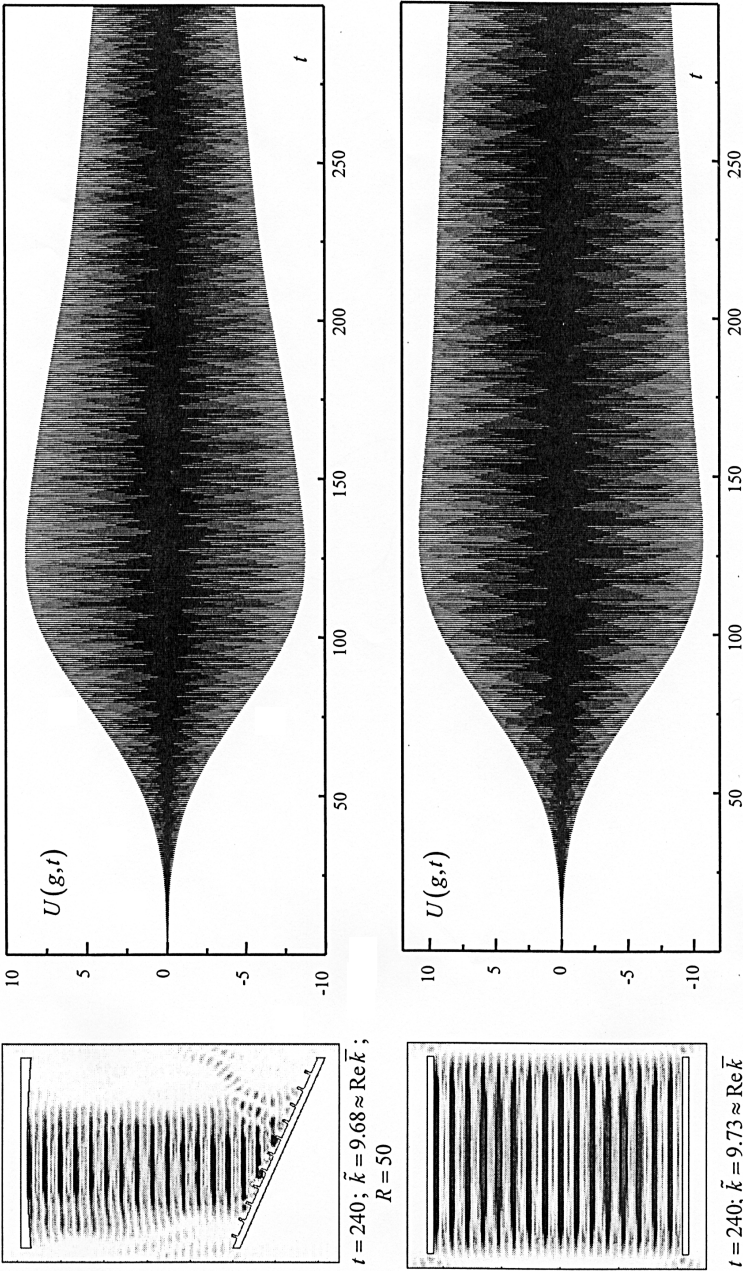


Figure 10. The high- Q $H_{0,1,32}$ -oscillations: $g = \{0; 9.85\}$.

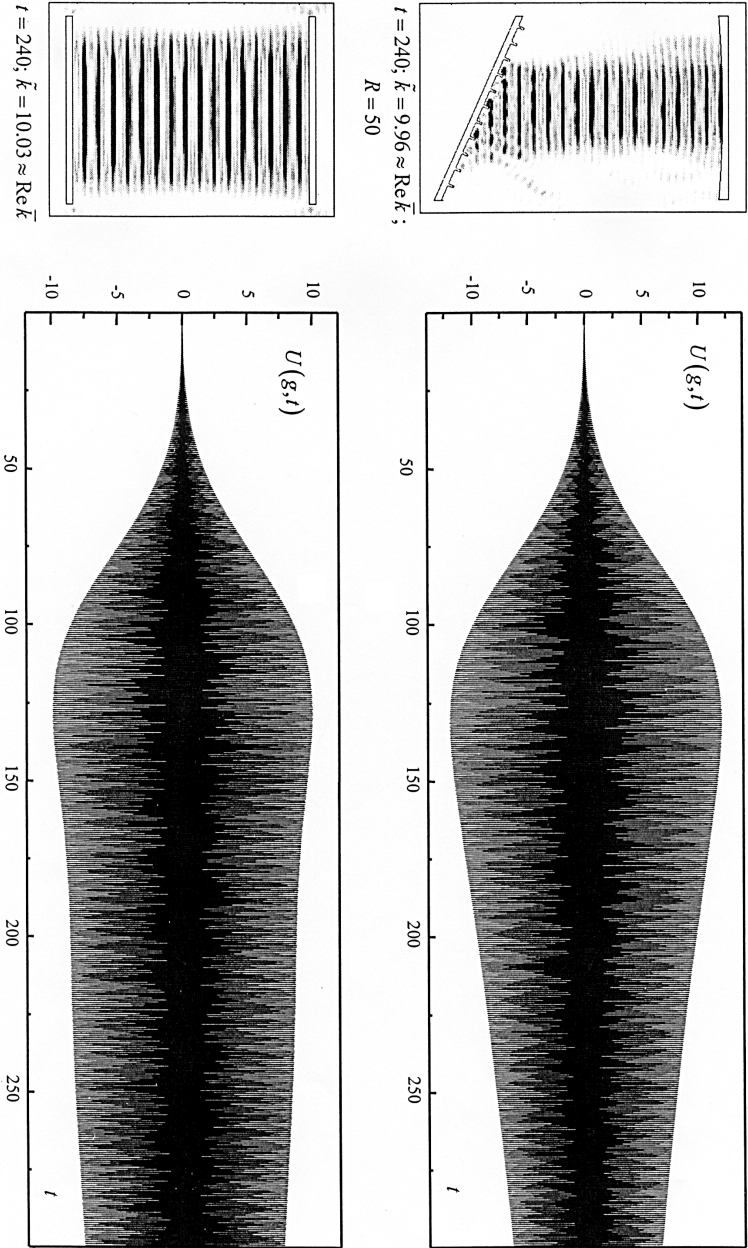


Figure 11. The high- Q $H_{0,1,33}$ -oscillations: $g = \{0; 9.85\}$.

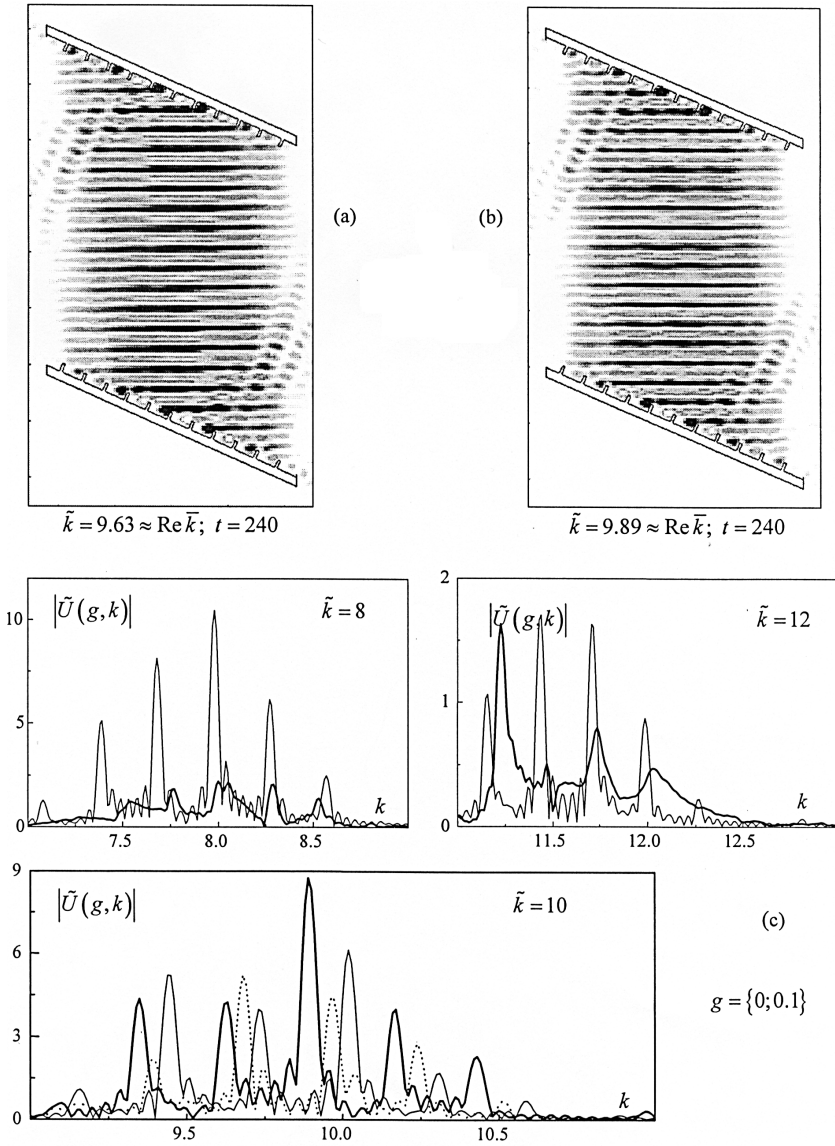


Figure 12. The high- Q $H_{0,1,32}$ - (a) and $H_{0,1,33}$ - (b) oscillations in the resonator with two selective mirrors. Spectral characteristics of the dispersive resonator and the Fabry-Perot resonator (thin lines) in the frequency range $7 \leq k \leq 13$ (c).

in the synthesis of single-mode resonator structures. A set of such mirrors (two, three or more) allows general geometry and size of an OR, Q -factor, configuration and spatial distribution of a field intensity to be varied almost arbitrarily.

4. CONCLUSIONS

According to [6], the nonspecular total (or near-total) reflection mode in periodic structures is connected with the excitation of natural free oscillations. Hence, the efficient selection of oscillations in an OR with gratings calls for a combination of resonant conditions for the original open quasi-optical system and the dispersive element involved. This problem is very complicated. It can be resolved adequately only in the framework of the complex approach, which utilizes a broad spectrum of methods and results of both the frequency domain and the time domain. Our paper, providing support for this view, will hopefully be found useful for further investigations.

REFERENCES

1. Weinstein, L. A., *Open Resonators and Open Waveguides*, Golem Press, Boulder, Colorado, 1969.
2. Taflove, A. and S. C. Hagness, *Computational Electrodynamics: the Finite-Difference Time-Domain Method*, Artech House, Boston, 2000.
3. Perov, A. O., Y. K. Sirenko, and E. Yaldiz, “‘Absorbing’ conditions for modeling of transients in open structures,” *Telecommunications and Radio Engineering*, Vol. 55, Nos. 6–7, 80–90, 2001.
4. Perov, A. O., Yu. K. Sirenko, and N. P. Yashina, “Explicit conditions for virtual boundaries in initial boundary value problems in the theory of wave scattering,” *Journal of Electromagnetic Waves and Applications*, Vol. 13, No. 10, 1343–1371, 1999.
5. Pazynin, V. L. and Y. K. Sirenko, “A two-dimensional model for pulse propagation in the physical environment: proper truncation of computational domain in the finite-difference method,” *Telecommunications and Radio Engineering*, Vol. 57, Nos. 2–3, 9–17, 2002.
6. Shestopalov, V. P., A. A. Kirilenko, S. A. Masalov, and Yu. K. Sirenko, *Resonance Wave Scattering*, Vol. 1, Diffraction Gratings, Kyiv, Naukova Dumka, 1986.

7. Shestopalov, V. P., L. N. Litvinenko, S. A. Masalov, and V. G. Sologub, *Wave Diffraction on Gratings*, Kharkov State University, Kharkov, 1973.
8. Petit, R. (ed.), *Electromagnetic Theory of Gratings*, Springer, New York, 1980.